Enhancing 1-Hexene Reactivity Under Inhibitive Temperatures Using Ozone

Caroline Smith Lewin, Olivier Herbinet, Frédérique Battin-Leclerc, Luc-Sy Tran, Guillaume Vanhove, Jérémy Bourgalais

Enhancing 1-Hexene Reactivity under Inhibitive Temperatures using Ozone

Caroline Smith Lewin[a], Olivier Herbinet[a], Frédérique Battin-Leclerc[a], Luc-Sy Tran[b], Guillaume Vanhove[b] and Jérémy Bourgalais[a,*]

[a]*Université de Lorraine, CNRS, LRGP, F-54000 Nancy, France*

[b]*Université Lille, CNRS, PC2A, F-59000 Lille, France*

KEYWORDS: Ozone; Jet-stirred Reactor; Kinetic Modeling; Gas Chromatography; Negative Temperature Coefficient.

---

*Corresponding author: Jérémy Bourgalais

e-mail: jeremy.bourgalais@cnrs.fr

ORCID: 0000-0003-4710-8943

ABSTRACT: This research delved into the oxidation chemistry of 1-hexene with and without the addition of O_3 within a 350 – 800 K temperature range using a near-atmospheric pressure jet-stirred reactor. Using gas chromatography and mass spectrometry, the products were identified, revealing O_3 ability to enhance fuel oxidation and enabling its significant conversion in typically inhibitive conditions (< 500 K and > 700 K). Due to the addition of O_3, an efficient fuel conversion is noticed at the lowest temperatures, while a significant fuel reactivity persists in the high temperature zone where the negative temperature coefficient behavior is almost fully suppresses. The addition of O_3 induces an increased production of aldehydes (formaldehyde, acetaldehyde, propanal, butanal and pentanal) and acids (pentanoic acid) at the lowest temperatures and amplifies the formation of several products (CO_2, CO, butene, butyl-oxirane, 2-butanone, ethylene, methanol, ethanol, furan, acrolein, acetone, propene, butadiene, methyloxirane, ethyloxirane, pentane, methylvinylketone) at higher temperatures. A significant concentration of ketohydroperoxides is also formed below 500 K. Our experimental findings, compared to the simulations of an updated kinetic model, suggest that ozonolysis at low temperatures and the interaction of O-atoms from the thermal decomposition of O_3 with oxidation products at high temperature are responsible of the fuel conversion enhancement by enriching the radical pool. The implications of this study spanning both combustion and atmospheric chemistry domains show that the incorporation of O_3 promises enhanced combustion fuel efficiency and strengthen its potential in optimizing fuel blends, pioneering combustion strategies, and pollution control.

INTRODUCTION

Plasma-assisted combustion offers potential advancements in the development of superior air-breathing engines. This is due to its ability to significantly change both kinetic and transport attributes, leading to improved ignition, better emission control, and stable flame [1]. Yet, achieving uniform plasmas in the high-pressure environments typical of combustion processes presents a challenge [2]. As a result, there is a growing interest in using ozone (O_3), an electrically produced and long-lasting species that can be introduced upstream of the combustion chamber. The presence of O_3 also facilitates low-temperature reactions, enabling fuel conversion at temperatures beneath traditional low-temperature combustion (LTC) conditions. This conversion happens either through O-atoms generated from O_3 thermal decomposition or via O_3-addition to the fuel skeleton, depending on the fuel molecular structure [3].

While oxidation by O-atoms mainly speeds up chain-branching reactions [4–8], ozonolysis initiate fuel conversion at ambient temperatures. This process yields different oxidation products, thereby altering the overall reaction network. Such changes can significantly influence fuel combustion properties. However, there is a limited amount of research that delves into the elementary reactions and resultant products of ozonolysis at combustion-relevant temperatures. This knowledge gap means that uncertainties persist in understanding the chemistry of O_3 in combustion, essential for enhancing emission control and efficiency in new technological designs. Existing experiments at combustion-relevant temperatures have mostly been limited to flow reactors using few reactants [9–12]. These efforts have given insights into kinetic mechanisms and preliminary modeling based on global ozonolysis reactions that qualitatively capture the profiles of the main products [8,10,12].

In the literature, 1-hexene (C_6H_{12}), is often proposed as a representative alkene component in gasoline surrogate fuels [13–15]. However, there is only one study about the reactions of this fuel with O_3 under combustion-relevant conditions. This was performed in an homogeneous charge compression ignition (HCCI) engine by reacting a variable fuel portion with O_3-containing air by Schöborn et al. [16]. These measurements indicate an increase in pressure and heat release in presence of O_3, as well as earlier ignition. There was also a notable decrease in particle emissions and an increase in combustion efficiency under elevated pressure and temperature conditions.

Our study explores the impact of O_3 on the oxidation of 1-hexene, known for its pronounced LTC chemistry [17], over a large temperature span (300—800 K). We found that O_3 does not just intensify oxidation but also alters the fuel temperature-driven reactivity; at both low (< 500 K) and high temperatures (> 700 K), thus eliminating the conventional restrictions of LTC. Our results highlight the potential of O_3 to counteract the negative temperature-coefficient (NTC) behavior usual in combustion, where reactivity decreases as the temperature increases [18,19]. Additionally, we show that the effect of O-atoms in O_3-driven oxidation differs from those in the oxidation of saturated fuels [5,20].

In this research, conducted using a Jet-Stirred Reactor (JSR), we identified and quantified main products and stable intermediates using gas chromatographs (GCs) and mass spectrometry (MS), both with and without O_3 introduction. Then our findings were compared with a kinetic model of 1-hexene oxidation from literature, updated in order to integrate global ozonolysis reactions. This allowed us to identify pivotal elementary processes when O_3 is incorporated.

The manuscript is structured into five sections:

(1&2) The first two present the experimental setup and the kinetic model used in this work.

(3) A section describing the experimental results confronted to the predictions of the kinetic model.

(4) A section presenting a kinetic analysis using the kinetic model at three relevant temperatures into a respective sub-section: (a) 400 K, the ozonolysis zone, (b) 650 K, the maximum of fuel conversion, (c) 750 K, the LTC minimum; a final sub-section on the impact of O-atoms at high temperature is closing the section.

(5) A conclusion summarizing the main results and take-home messages.

EXPERIMENTAL METHOD

The JSR experimental setup and the GC method used to quantify oxidation products are similar to those mentioned in earlier studies. Therefore, we will provide only a brief summary with details unique to this study. For more in-depth details on the GC method, refer to the JSR study of 1-hexene LTC performed by Meng et al. [17]. Specifics regarding the use of JSR with O_3 are available in Smith Lewin et al. [10].

We conducted the oxidation of 1-hexene with or without O_3 in a near-atmospheric JSR that is heated by shaped electric resistances. This spherical reactor, made from fused silica with a volume of around 81.2 cm^3, ensures stable temperature and pressure conditions [21]. We continuously fed gas mixtures consisting of 1-hexene, O_2, and optionally O_3, into the reactor. To stabilize temperature fluctuations in the JSR due to exothermic reactions, we introduced a significant amount of inert helium gas. The reactor temperature was measured using a K-type thermocouple positioned in a glass finger close to the JSR center indicating a temperature uncertainty of around

105 1%.[21] For all experiments, we kept the pressure, equivalence ratio, and inlet mole fraction of 1-
106 hexene constant at 800 Torr (1.067 kPa), 0.5, and 0.01. The flow rates were adjusted according to
107 temperature, ensuring a constant residence time of 2.0 s (without O_3) or 2.5 s (with O_3). The
108 increased residence time for the case with O_3 is explained by the need to perform more experiments
109 in the very low temperature region, which leads to higher flow rates into the JSR than the one
110 considered maximum ideally (2 NL/min). However, simulations using 2 and 2.5 s as residence
111 time for the case without O_3 showed no significant changes. When initiating oxidation with O_3,
112 we used an O_3 generator to impose a mole fraction of 1,000 ppm that was blended with the fuel
113 just before entering the JSR. Since O_3 is highly reactive even at room temperatures, the reaction
114 time between the fuel and O_3 has been minimized before the reactor preheating stage by mixing
115 the reactants just at the entrance.[10]

116 The gases resulting from oxidation in the JSR were directed through heated stainless-steel tubes
117 to three GCs to quantify the stable and intermediate products. The first GC, equipped with a
118 Carbosphere-packed column and a thermal conductivity detector (TCD), measures lightweight and
119 permanent gases. The second GC, paired with a Q-Bond capillary column and a flame ionization
120 detector (FID) preceded by a methanizer, was used primarily to quantify organic compounds
121 containing from 1 to 5 carbon atoms. This methanizer contains a hydrogenation nickel catalyst. A
122 third GC equipped with a HP-5 column and an FID was used to quantify organic compounds
123 containing more than 5 carbon atoms. To identify species, a GC with either the Q-Bond or the HP-
124 5 capillary columns was paired with a quadrupole mass spectrometer, achieving ion generation
125 using electron ionization at 70 eV. The identification of the species was determined by comparing
126 the fragmentation pattern of each peak, associated with a specific retention time, to the NIST
127 database [22].

The calibration factors for both GC-FIDs were derived from injection of the fuel in non-reactive conditions. For the GC with the HP-5 column (without the methanizer), the effective carbon number (ECN) method [23] was employed to obtain the mole fractions of the detected species in comparison to the one of the fuel. The estimated uncertainties were ±5% for the fuel and about ±10% for species quantified using conversion factors from the fuel mole fraction. We calibrated the TCD using gaseous standards from Air Liquide for O_2 with the estimated uncertainty of ±5%.

The mole fractions of all the quantified products are provided in the excel spreadsheet in Supplementary Information (SI).

KINETIC MODEL

The detailed kinetic model used in this work is a upspring of the kinetic model developed and validated by Meng et al.[17] to simulate the JSR oxidation of 1-hexene. The new kinetic model includes 1134 species and 4887 reactions and is provided in SI along with its thermochemical data. In this work, we added an O_3 sub-mechanism [24] to model the O_3-initiated oxidation experiments. Due to a lack of information regarding the details of the elementary reactions following ozonolysis and their kinetic parameters, we implemented 8 lumped reactions using the same kinetic parameters taken from Avzanovia et al. [25] for 1-hexene global ozonolysis reaction (A=1.39E+09 cm^3 $mole^{-1}$ s^{-1}, n=0.00, Ea=3140.5 cal $mole^{-1}$) assuming the same contribution of the 8 channels. The following reactions, (1) to (8), which lump the several elementary steps involving Criegee intermediates (CIs), were written to model the detected products, pentanal (C_4H_9CHO), formaldehyde (HCHO), 2-hydroxypentanal (C_4H_8OHCHO), pentanoic acid (C_4H_9COOH), butene (C_4H_8), butanal (C_3H_7CHO), and other stable products:

$C_6H_{12} + O_3 \leftrightarrow C_4H_9CHO + OH + HCO$ (1)

$C_6H_{12} + O_3 \leftrightarrow C_4H_9CHO + CO + H_2O$ (2)

$C_6H_{12} + O_3 \leftrightarrow C_4H_9CHO + CO_2 + H + H$ (3)

$C_6H_{12} + O_3 \leftrightarrow C_4H_9CHO + CO_2 + H_2$ (4)

$C_6H_{12} + O_3 \leftrightarrow HCHO + C_4H_8OHCHO$ (5)

$C_6H_{12} + O_3 \leftrightarrow HCHO + C_4H_9COOH$ (6)

$C_6H_{12} + O_3 \leftrightarrow HCHO + C_4H_8 + CO_2 + H_2$ (7)

$C_6H_{12} + O_3 \leftrightarrow HCHO + C_3H_7CHO + CO + H_2$ (8).

The presence of formaldehyde and pentanal aligns with the typical ozonolysis mechanism, which starts with O_3 adding to the double bond of 1-hexene, resulting in a primary ozonide (POZ), known as 4-butyl-1,2,3-trioxolane. For 1-hexene, the POZ can break down into two reactive CIs: CH_2OO and C_4H_9CHOO, with formaldehyde and pentanal as their co-products (see Fig. 1). Further unimolecular CI decomposition, isomerization, bimolecular reactions lead to other significant species such as butanal, butene, acetaldehyde, propanal, pentanoic acid, butyl-oxirane, and 2-butanone considered in the globalized reactions 1 to 8. The detailed analysis of these complex chemical pathways at very low temperatures is currently the subject of a specific study.[26]

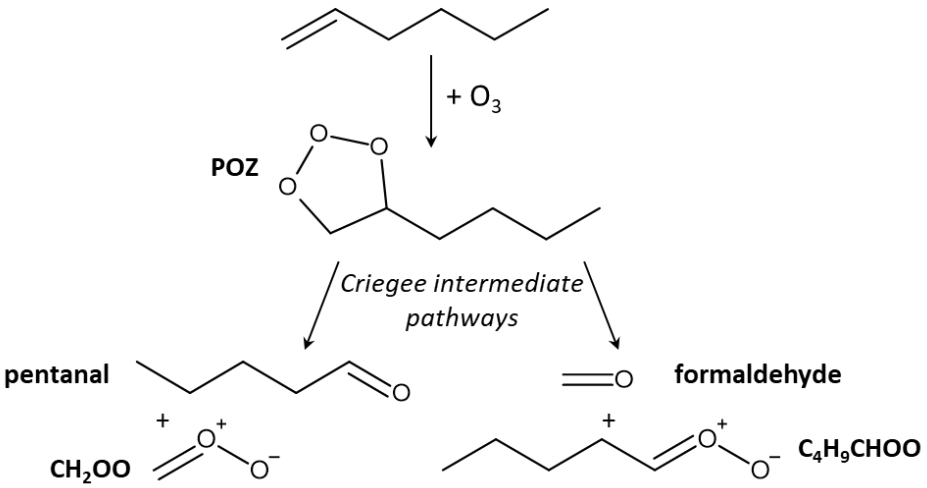

Figure 1. 1-hexene ozonolysis scheme

Using the CHEMKINPro software [27], we modeled the 1-hexene oxidation without O_3 considering a perfectly stirred reactor (PSR), typical for JSR models, given that the residence time in the preheating zone can be neglected compared to that in the JSR. For the O_3-assisted oxidation, we included two plug flow reactors (PFR) before the JSR, replicating the two-stage experimental preheating zone. Earlier research emphasized the significance of modeling this preheating section, noting that O_3 partially converts in this area.[10,28,29] According to simulations (see Fig. S1), out of the 1,000 ppm injected at 350 K, 149 and 26 ppm of O_3 enter the second PFR and the PSR, respectively, whereas those numbers decrease to 20 and 0 ppm at 700 K. PFR simulations used the same dimensions and temperatures as the preheating quartz tube preceding the JSR in experiments.

EXPERIMENTAL RESULTS COMPARED TO KINETIC PREDICTIONS

The mole fraction profile of 1-hexene resulting from its oxidation, both with and without O_3, are shown in Fig. 2. Carbon balance varied from 78% to 101% for the case without O_3 and from 70%

to 90% for the O_3-assisted oxidation case. Those values are included in the tabulated experimental data in the SI. The experimental data without O_3 aligns well with the earlier ones by Meng et al. [17] as illustrated in Fig. S2 in SI. The O_3 mole fraction is not shown because it is nearly 0 at 350 K. Based on Fig. 2, introducing a small amount of O_3 enables the fuel to start reacting at room temperature. Between temperatures from 300 to 550 K, about 20% of the fuel is converted when O_3 is incorporated. Although the temperature of the start of the LTC remains about the same at 550 K, the conversion rate is still 20% higher at the peak conversion temperature of 650 K. Notably, in the NTC region (temperatures exceeding 650 K), where the fuel conversion drops sharply from 44% to 10% without O_3, the conversion rate remains significantly higher, above 50% in presence of O_3. This is near the highest conversion rate observed at 650 K in the LTC range in ozone-less conditions. The addition of O_3 does not cause a shift of the NTC region. The difference in mole fractions between scenarios with and without O_3 amplifies to 44% at 750 K, which is more than the 20% increase seen at lower temperatures. These findings indicate that besides just enhancing oxidation, O_3 also triggers fuel conversion under conditions that typically inhibit it under standard oxidation conditions. This starts from room temperature and extends to higher temperatures, diminishing the usual NTC patterns, until it reaches the high temperature zone (above 800 K) where all the fuel gets consumed. A similar effect was intuited in the literature, although it was not as obvious as the one observed in this study [30,31].

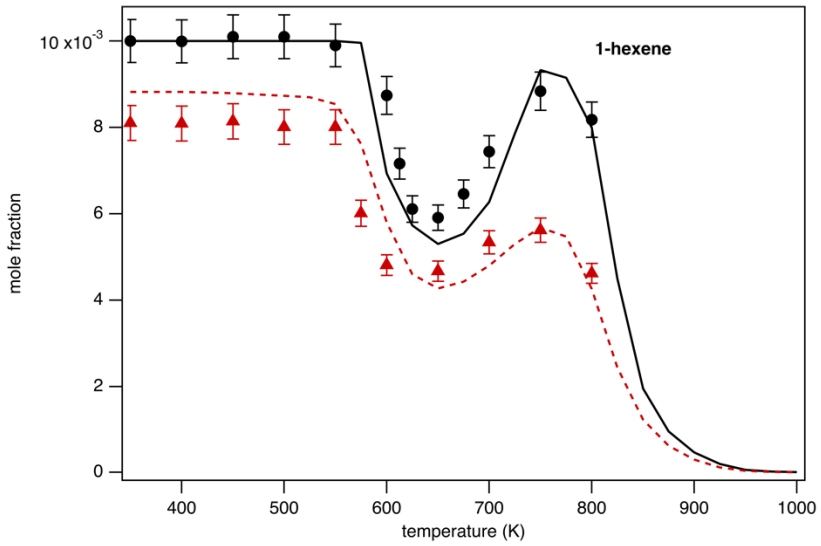

Figure 2. Comparison of experimental (symbols) and predicted (lines) mole fraction profiles for the conventional (black dots and solid lines) and O_3-initiated (red triangles and dashed lines) oxidation of 1-hexene. The condition of pressure, equivalence ratio, and inlet mole fraction of 1-hexene was kept constant at 800 Torr (1.067 kPa), 0.5, and 0.01 respectively. The residence time was 2.0 s (without O_3) or 2.5 s (with O_3).

Fig. 3 displays the mole fraction of all the observed products produced during 1-hexene oxidation below 500 K as determined by GC measurements. Without O_3, the results for the four key products, namely CO, formaldehyde, CO_2, and pentanal generally align well with the previous findings of Meng et al. [17] as shown in Fig. S2. However, we observed that the mole fractions for formaldehyde and pentanal are consistently lower than Meng et al.'s data. In contrast, the mole fraction of CO_2 at high temperatures is higher than Meng et al.'s results.

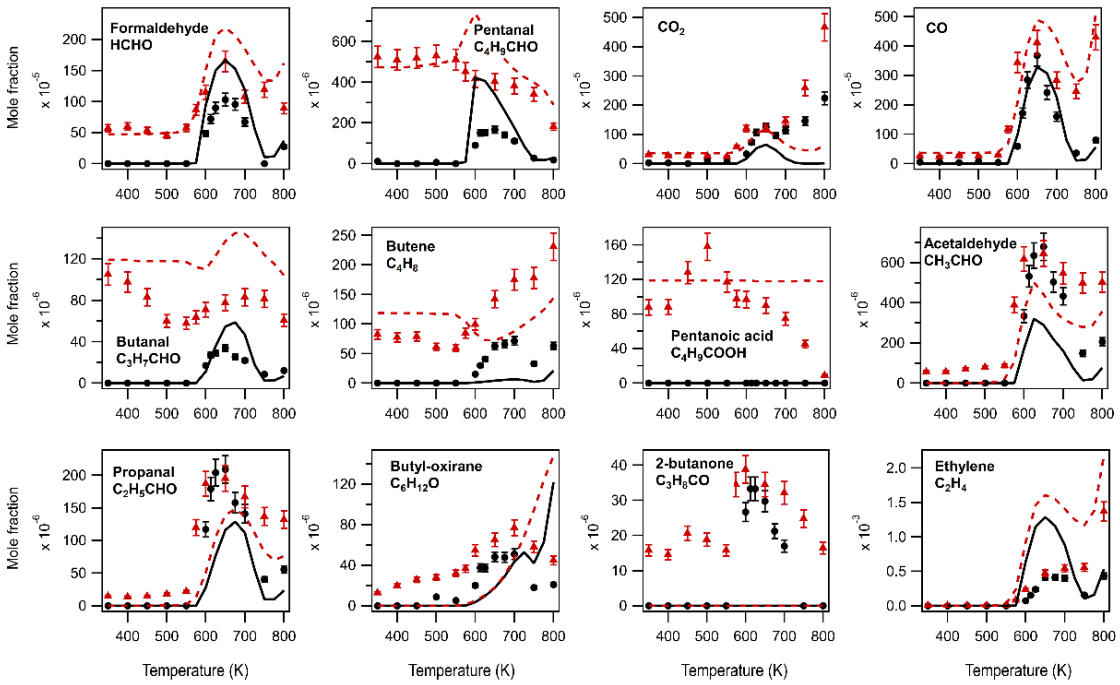
Formaldehyde
HCHO
Pentanal
C_4H_9CHO
CO_2
CO
Butanal
C_3H_7CHO
Butene
C_4H_8
Pentanoic acid
C_4H_9COOH
Acetaldehyde
CH_3CHO
Propanal
C_2H_5CHO
Butyl-oxirane
$C_6H_{12}O$
2-butanone
C_3H_8CO
Ethylene
C_2H_4
Mole fraction
Temperature (K)

213

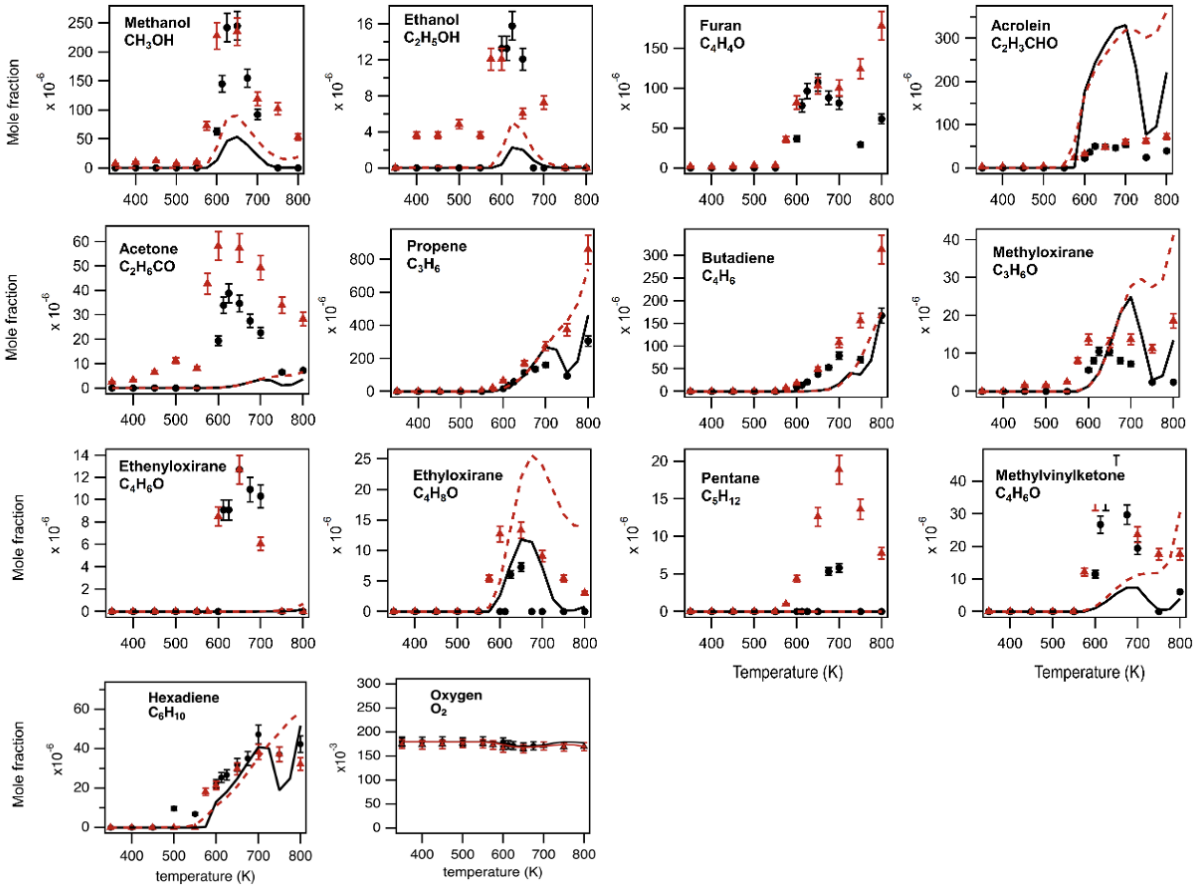
Methanol
CH_3OH
Ethanol
C_2H_5OH
Furan
C_4H_4O
Acrolein
C_2H_3CHO
Acetone
C_2H_6CO
Propene
C_3H_6
Butadiene
C_4H_6
Methyloxirane
C_3H_6O
Ethenyloxirane
C_4H_6O
Ethyloxirane
C_4H_8O
Pentane
C_5H_{12}
Methylvinylketone
C_4H_6O
Hexadiene
C_6H_{10}
Oxygen
O_2
Mole fraction
temperature (K)

214

Figure 3. Comparison of experimental and predicted mole fraction profiles of all the observed products for the conventional (black dots and solid lines) and O_3-initiated (red triangles and dashed lines) oxidation of 1-hexene. The condition of pressure, equivalence ratio, and inlet mole fraction of 1-hexene was kept constant at 800 Torr (1.067 kPa), 0.5, and 0.01 respectively. The residence time was 2.0 s (without O_3) or 2.5 s (with O_3).

According to Fig. 3, with O_3 at temperatures below 600 K, the dominant products are formaldehyde (around 500 ppm) and pentanal (roughly 500 ppm). CO and CO_2 become prevalent at higher temperatures. Significant amounts (measured in ppm) of other species were detected, including butanal, butene, acetaldehyde, propanal, pentanoic acid, butyl-oxirane, 2-butanone, and ethylene. Notably, pentanoic acid is unique in that it is not formed during standard oxidation but appears only when O_3 is added across all temperatures studied.

Additional minor species present at low temperatures were also identified using GCs: these include methanol, ethanol, furan, acrolein, and acetone. Note that the discrepancy regarding methanol between the model and the experimental data, which is a significant byproduct (approximately 200 ppm), had already been observed during the oxidation of 1-hexene.[17] The co-elution of methanol and acetaldehyde, which is also a main species in the LTC region (see Fig. 3), likely contributed to a degradation in the accuracy of both measurement species. At higher temperatures, other detected minor species include propene, 1,3-butadiene, methyloxirane, ethenyloxirane, ethyloxirane, pentane, methylvinylketone, and 2,4-hexadiene. In summary, adding O_3 boosts the production of carbonyls and acids, especially at cooler temperatures. Additionally, there is a notable increase in CO production at higher temperatures, with it being four times higher at 800 K.

When we compare the experimental mole fraction of fuel and products with predictions from the kinetic model (as seen in Fig. 3), they align fairly well at low temperature for the main species.

The proposed model allows the fuel conversion trends to be well simulated at both low and high temperatures. Looking closely at Fig. 3, the inlet mole fractions of formaldehyde and pentanal from model simulations agree well with experimental data at low temperatures, at higher temperature the model overpredict the mole fraction of both species, which could also be seen under conventional oxidation conditions. The CO and CO_2 mole fraction profiles are also reasonably reproduced by the model at low temperature, while CO_2 is clearly underestimated at the highest temperatures. Butanal mole fraction at low temperatures is overestimated, while butene profile is reasonably predicted assuming a 100 K shift, mirroring the trend in conventional oxidation. Pentanoic acid mole fraction remains stable, even with recent modeling insights into its oxidation kinetics [32]. Though the order of magnitude is accurate, the maximum deviation is about three times over the entire temperature range.

For minor species like acetaldehyde, propanal, and butyl-oxirane, the model predictions are reasonable at high temperature, but their mole fractions at low temperatures are slightly underestimated. The notable deviations in the prediction of butyl-oxirane highlights the limitation of the global reactions for ozonolysis as could be a product of the isomerization of the CI formed by ozonolysis (see section regarding the kinetic model) for which no kinetic data is available in the literature, explaining that the kinetic model does not produce butyl-oxirane at low temperature. The production of 2-butanone is the worst predicted one because no formation reaction for this ketone was identified, even if experimental data show ppm-level mole fractions, even at the lowest temperatures. In general, the kinetic model predictions fairly match with the experimental mole fraction profiles of the main species at low temperature considering that only global ozonolysis reactions have been implemented due to a lack of kinetic data in literature. Especially the trend of O_3 effect is well captured for the fuel. However, it is essential to approach the interpretation of the

modeling results with caution, recognizing the need for further validation in a near future especially across different experimental conditions to address the robustness of the model.

KINETIC ANALYSIS OF THE DIFFERENT TEMPERATURE ZONE

This part describes the kinetic analysis based on the present model in the three considered temperature zone and discuss the effect of O-atoms generated by O_3 decomposition.

At 400 K, the ozonolysis zone

Fig. 4 displays a flow rate analysis at 400 K. At this temperature, the primary reactions involve the fuel interacting with O_3, yielding distinct ozonolysis products.

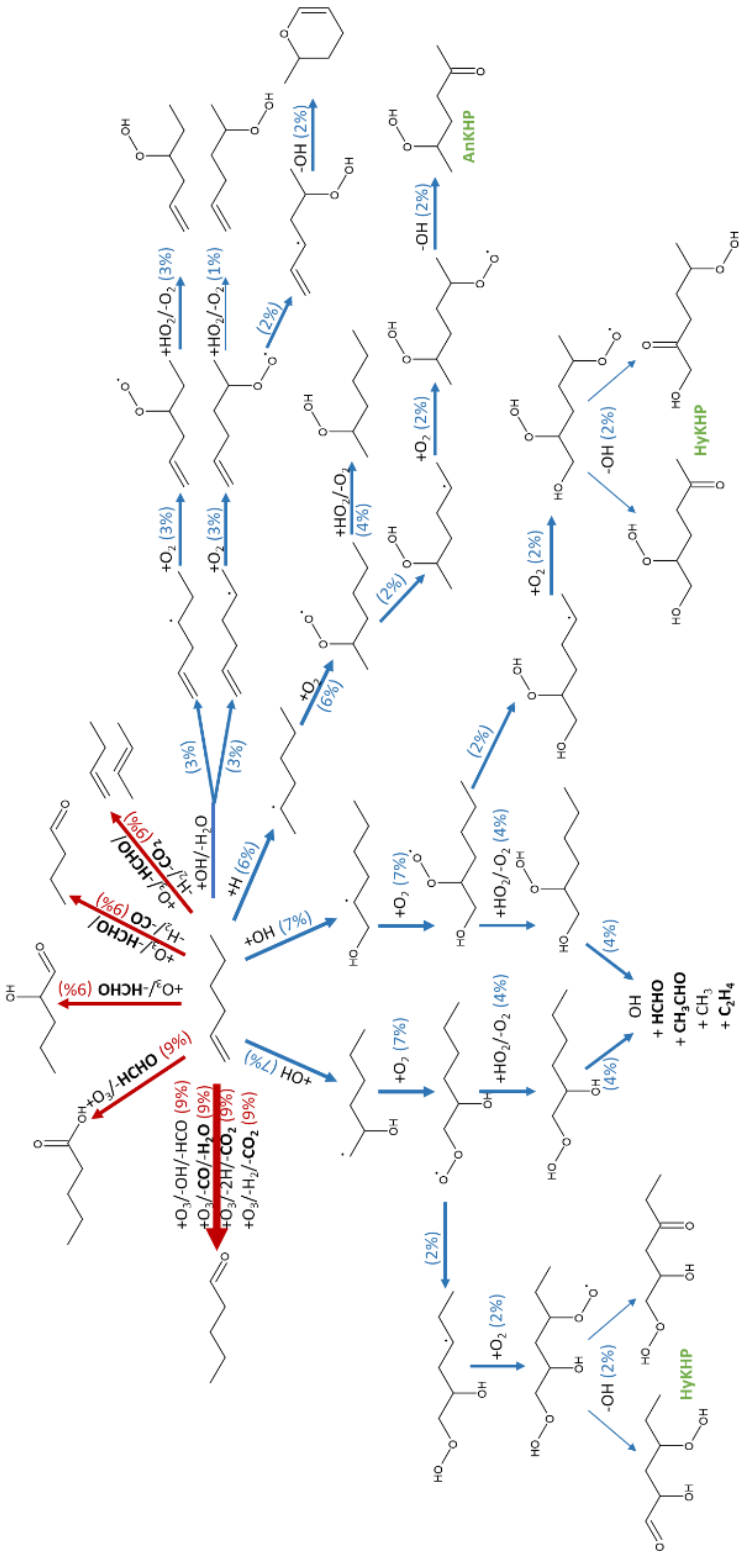

Figure 4. Flow rate analysis for 1-hexene oxidation assisted by O_3 (1,000 ppm), at 400 K under the current experimental conditions of Fig. 2, obtained by simulations. Each arrow denotes the percentage of fuel consumption in the corresponding pathway. For the sake of clarity, only pathways above 1% are displayed.

As shown in Fig. 4, at 400 K ozonolysis reactions (reactions (1-8)) consume 72% of the fuel. The sensitivity analysis on the fuel in Fig. S3 supports this observation, emphasizing the primary importance of reaction between O_3 and 1-hexene. The remaining conversion is due to reaction pathways related to the conventional low-temperature oxidation kinetics, initiated by reactions between the fuel and radicals that are produced through the ozonolysis channels.

Another interesting observation based on Fig. 4 is that the addition of O_3 induces the formation of alkenyl ketohydroperoxides (AnKHP) and hydroxyl ketohydroperoxides (HyKHP) at temperature as low as 400 K. Those KHPs were detected and characterized experimentally in Smith Lewin et al.[26]: a typical mass spectrum registered at 400 K showing the peaks of KHPs is given in Fig. S4. Fig. 5 presents the simulated mole fraction profiles of AnKHP and HyKHP and highlights that the formation of KHPs starts to be significant just above 400 K. Around 20-25% of the amount of KHPs formed in the LTC region is reached below 500 K. However, due to the needed activation energy, around 42 kcal/mol, despite the formation from 400 K, HyKHP and AnKHP cannot decompose significantly before 550 K. Consequently, the acceleration of the reactivity due to the branching step cannot occur before this temperature. The 0.7 AnKHP/HyKHP ratio predicted at 400 K is in good agreement with the experimental ~1.0 AnKHP/HyKHP ratio at 400 K (see the inserts in Fig. 5). This value is based on experimental mole fractions calculated from the mass spectrum signals in Fig. S4 using the method described in Bourgalais et al. [33].

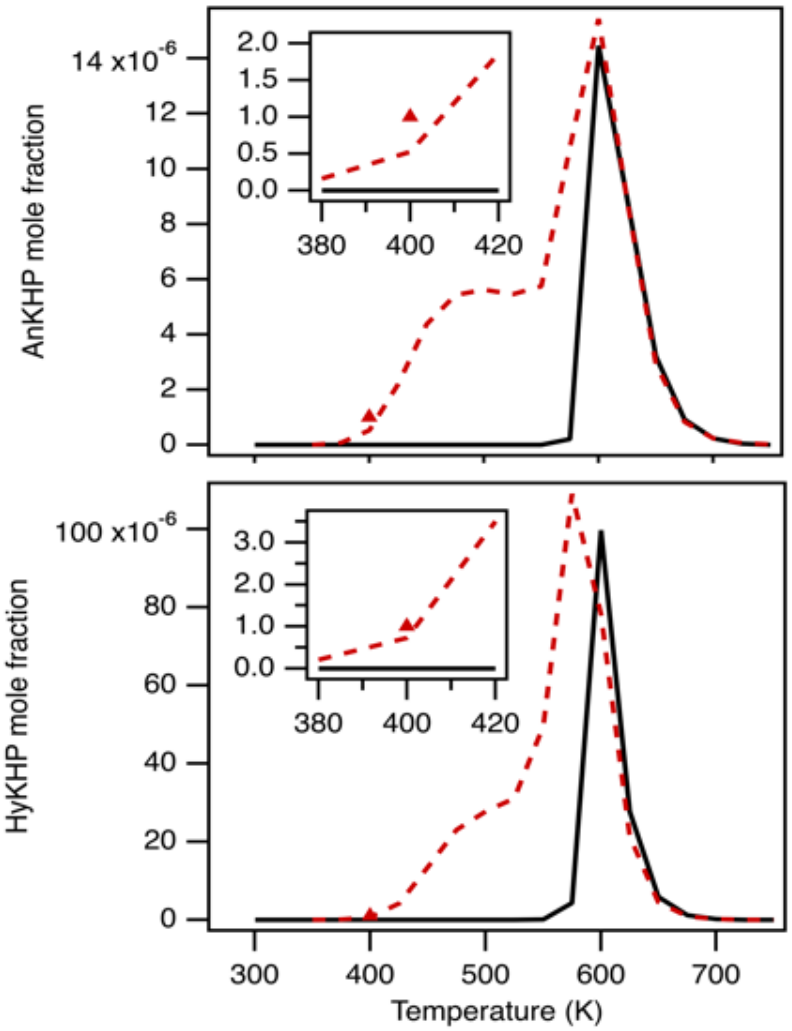

Figure 5. Simulated mole fractions of AnKHP (upper panel) and HyKHP (lower panel) under the experimental conditions of Fig. 2. Black and red lines correspond to the cases without and with O_3, respectively. The red dots are experimental mole fraction calculated from Fig. S3.

At 650 K, the maximum of fuel conversion

A second flow rate analysis, at 650 K, with 1,000 ppm and without O_3, is shown in Figure S6 and aligns with the pathway distribution reported by Meng et al. [17]. The sensitivity analysis shown in Fig. 6 on fuel mole fraction, denoted as C6H12Z-1, shows reactions ordered by importance for the case with O_3 and does not indicate much difference with or without O_3. It suggests that the

enhanced fuel conversion observed in Fig. 2 results from the same reaction pathways but with a slight sensitivity boost of some reactions between the fuel and radicals like H and OH in the presence of O_3.

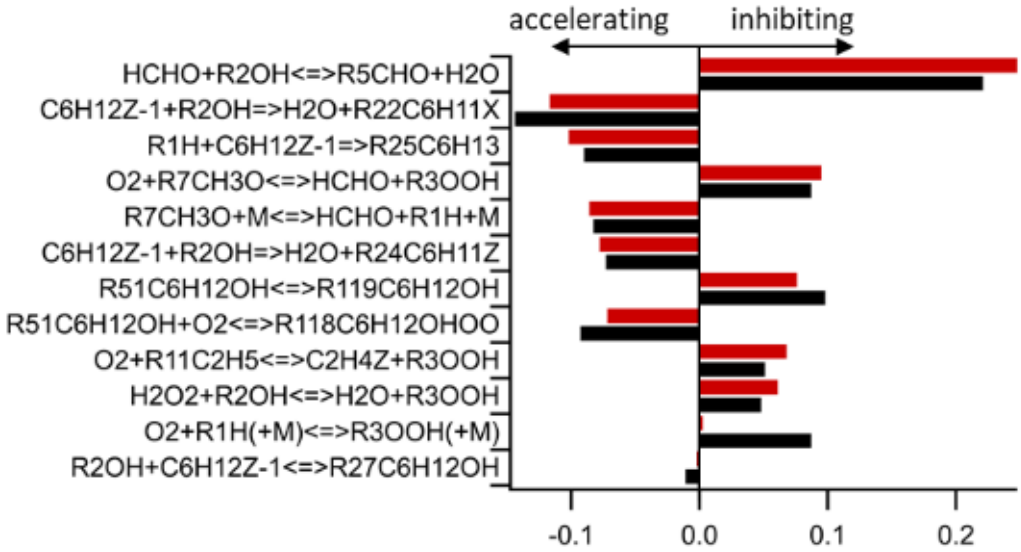

Figure 6. Sensitivity analysis at 650 K for the fuel mole fraction without (black) and with O_3 (red) under the experimental conditions of Fig. 2.

This increased sensitivity stems from the growing radical pool as the temperature increases due to the thermal decomposition of O_3 into O-atoms and O_2. Fig. 7 shows predictions from the kinetic model under our current experimental conditions of the ratio of the O_3 flux going through the O-formation pathway in the total O_3 consumed flux. The thermal decomposition of O_3 competes with ozonolysis starting from around 550 K, a temperature about 100 K higher than that the start of thermal decomposition of neat O_3 (450 K in Fig. 7).

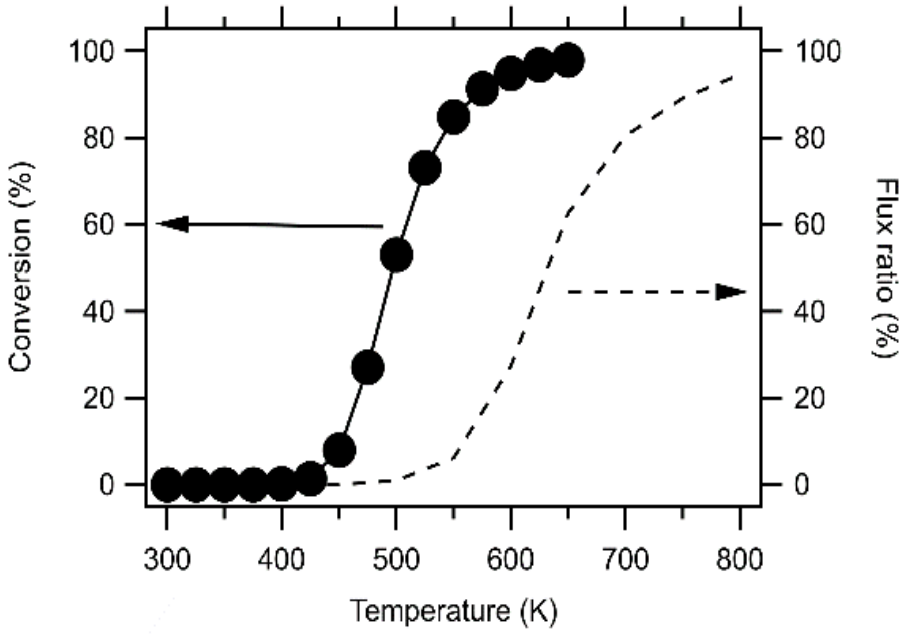

317

318 *Figure 7. Comparison between the thermal decomposition of neat O_3 in the JSR [10] (black dots) compared to the predictions of*
319 *the ratio of O_3 flux leading to the formation of O-atoms in the total O_3 flux consumed under the experimental conditions of Fig. 2*
320 *(dotted line).*

321

322 The predictions of the kinetic model show that the thermal decomposition of O_3 becomes more
323 significant than the O_3 direct addition to the fuel unsaturation only above 600 K. However, one
324 should note that even if 40% of O_3 reacts with the fuel at 650 K, this flux corresponds to less than
325 1% for the fuel consumption, explaining why no ozonolysis reaction appears in Fig. S5.

326

327 ***At 750 K, the LTC minimum***

328 The impact of thermal decomposition of O_3 is anticipated to be more pronounced at elevated
329 temperatures, with more than 90% of O_3 resulting in O-atoms at 750 K, as depicted in Fig. 7. A
330 surge in the radical mole fractions is observed from 550 K, with an increase by up to ten times of
331 the radical mole fractions at 750 K, as illustrated in Fig. S6. Consequently, the sensitivity analysis

for the fuel mole fraction displayed in Fig. S7, emphasizes that the most sensitive reactions remain quite the same at both 650 K and 750 K when O_3 is introduced, while they significantly differ in absence of O_3. Additionally, we can notice that the sensitivity coefficients at 750 K are significantly larger in the presence of O_3 than without it. The fact that the inclusion of O_3 makes the sensitivity coefficients at 750 K to align closely with those at 650 K is consistent with the near-constant fuel conversion with O_3 within the NTC region observed in Fig. 2. However, at 750 K, the chemical pathways of fuel consumption are very much the same with and without O_3, as illustrated in Fig. S8.

The impact of O-atoms

The flow rate analysis in Fig. 8 shows that the thermal decomposition of O_3 into $O+O_2$ initiates radical reactions promoting fuel conversion. Predominantly, 48.5% of O-atoms react with the fuel by H-abstraction, which results in the formation of OH radicals along with mainly allylic radicals. However, O + RH = OH + R represents only less than 1% of both the fuel consumption and the OH formation. Most of the fuel consumption by H-abstraction is achieved via reactions with H and OH radicals (see Fig. S8).

The flow rate analysis in Fig. 8 shows that the thermal decomposition of O_3 into $O+O_2$ initiates radical reactions promoting the fuel conversion. Predominantly, 48.5% of O-atoms react with the fuel by H-abstraction, which results in the formation of OH radicals along with mainly C_6 allylic radicals. However, O + RH = OH + R represents only less than 1% of both the fuel consumption and the OH formation. Most of the fuel consumption by H-abstraction is achieved via reactions

with OH (45 %) and OOH (2.9%) radicals, as well as H-atoms (4.3%), as it is shown in the last flow rate analysis for 1-hexene consumption made at 750 K and displayed in Fig. S8.

The remaining O-atoms engage in reactions with formaldehyde HCHO (11.7%) and C_2H_4 (6.3%), producing CHO + OH and CH_3 + CHO, respectively. The CHO radicals primarily react with O_2, leading to the formation of OOH + CO, which accounts for the rise in the OOH radical mole fraction, as observed in Fig. S8. This process is also the predominant consumption route for O_2.

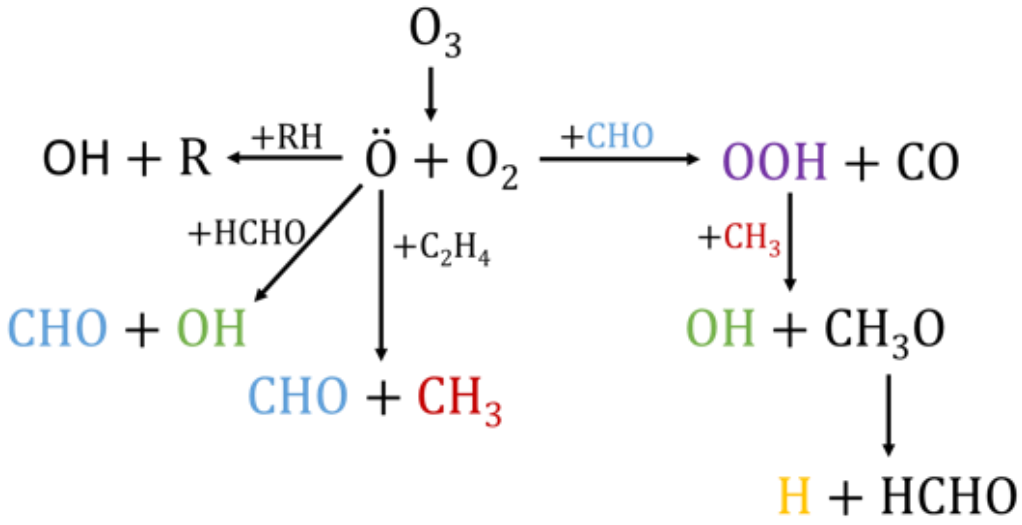

Figure 8. The important reactions initiated by the thermal decomposition of O_3 at 750 K.

While a significant portion of OOH (44%) recombines to yield H_2O_2+O_2, a notable amount of OOH (7.1%) also reacts with CH_3 radical, producing OH + CH_3O. This accounts as one of the main sources of OH: 6% at 750 K. It is interesting to compare this value to that coming from the decomposition of H_2O_2 into OH+OH, which accounts for 4.5% of OH formation at 750 K. The interaction of OOH with CH_3 intensifies when O_3 is introduced, primarily because O-atoms react by addition on C_2H_4, generating CHO and CH_3 radicals. The major formation of H-atoms (45%) occurs through the decomposition of CH_3O radicals, which results in H + HCHO. This elucidates

the gradual increase in H + fuel reactions observed from 650 K to 750 K in both flow rate and sensitivity analyses.

In summary, the observed decrease of the NTC behavior in this study does not predominantly stem from the conventional H-abstraction from RH by the O-atoms produced by O_3 decomposition. As an additional channel, O-atoms, when reacting with C_2H_4 and HCHO boost the formation of H-atoms and, OH and OOH radicals.

CONCLUSION

This work shows that O_3 triggers fuel conversion under conditions that typically inhibit oxidation, ranging from room temperature to higher temperatures. This process effectively diminishes the NTC behavior and continues until reaching a high-temperature phase (> 800 K) where all the fuel is consumed. The inclusion of O_3 fosters a significant production of aldehydes and pentanoic acid from 400 K, consistent with the ozonolysis mechanism. A significant concentration of KHPs is also formed between 400 – 500 K.

The model predictions align reasonably with the observed mole fraction profiles of major species considering that the O_3-related chemistry has been described in the kinetic model using global ozonolysis reactions due to a lack of kinetic information in the literature. However, more thorough theoretical kinetic studies on ozonolysis-related reactions would be required to implement more accurate mechanisms and improve the predictions. We hope these experimental data will stimulate future theoretical studies for the validation of kinetic parameters. In addition to the O-atom production by O_3 decomposition, we discerned that the observed diminution of NTC behavior is

mainly attributed to the O-atoms interacting with C_2H_4 and formaldehyde leading to a boost of the population of H and OH radicals.

The results suggest that the inclusion of O_3 can enable efficient molecule conversion across a wide temperature range, overcoming efficiently the usual reactivity barriers seen with NTC behavior. This demonstrates even more the interest of using O_3 as an oxidant to improve fuel combustion efficiency. This knowledge could influence fuel blend optimization, the development of novel combustion techniques working at extremely low temperature, and better pollution control in combustion systems.

SUPPLEMENTARY INFORMATION

Experimental data under tabulated format, reaction mechanism and thermochemical data files under CHEMKIN format, additional description of experimental data and simulation results.

ACKNOWLEDGMENT

This work was performed using HPC resources from the EXPLOR centre hosted by the University of Lorraine (Project: 2021EXTXX2356).

REFERENCES

(1) Ju, Y.; Sun, W. Plasma Assisted Combustion: Dynamics and Chemistry. *Progress in Energy and Combustion Science* 2015, *48*, 21–83. https://doi.org/10.1016/j.pecs.2014.12.002.
(2) Sun, W.; Ju, Y. 2. Nonequilibrium Plasma-Assisted Combustion: A Review of Recent Progress. 2013.
(3) Sun, W.; Gao, X.; Wu, B.; Ombrello, T. The Effect of Ozone Addition on Combustion: Kinetics and Dynamics. *Progress in Energy and Combustion Science* 2019, *73*, 1–25. https://doi.org/10.1016/j.pecs.2019.02.002.

(4) Liu, B.; Zhu, Q.; Zhu, L.; Hu, Z.; Xu, Q.; Wang, Z. Ozone-Initiated Low-Temperature Oxidation of Two Propanol Isomers: Revealing the Effects of Ö/ȮH Atoms/Radicals. *Combustion and Flame* 2023, *256*, 112956. https://doi.org/10.1016/j.combustflame.2023.112956.
(5) Zhu, L.; Xu, Q.; Xie, C.; Liu, B.; Wang, H.; Panigrahy, S.; Curran, H.; Wang, Z. Chemical Insight into the Ozone-Assisted Low-Temperature Oxidation of Propane. *Combustion and Flame* 2023, *254*, 112814. https://doi.org/10.1016/j.combustflame.2023.112814.
(6) Liao, W.; Chu, Z.; Wang, Y.; Yang, B. A Kinetic Investigation on Low-Temperature Ignition of Propane with Ozone Addition in an RCM. *Proceedings of the Combustion Institute* 2023, *39* (1), 395–403. https://doi.org/10.1016/j.proci.2022.07.261.
(7) Kaczmarek, D.; Rudolph, C.; Atakan, B.; Kasper, T. Kinetic Investigation of the Ozone-Assisted Partial Oxidation of Fuel-Rich Natural Gas Mixtures at Elevated Pressure. *Proceedings of the Combustion Institute* 2023, *39* (1), 211–221. https://doi.org/10.1016/j.proci.2022.07.195.
(8) Panaget, T.; Potier, K.; Batut, S.; Lahccen, A.; Fenard, Y.; Pillier, L.; Vanhove, G. How Ozone Affects the Product Distribution inside Cool Flames of Diethyl Ether. *Proceedings of the Combustion Institute* 2023, *39* (1), 325–333.
(9) Conrad, A. R.; Hansen, N.; Jasper, A. W.; Thomason, N. K.; Hidaldo-Rodrigues, L.; Treshock, S. P.; Popolan-Vaida, D. M. Identification of the Acetaldehyde Oxide Criegee Intermediate Reaction Network in the Ozone-Assisted Low-Temperature Oxidation of *Trans* -2-Butene. *Phys. Chem. Chem. Phys.* 2021, *23* (41), 23554–23566. https://doi.org/10.1039/D1CP03126K.
(10) Smith Lewin, C.; Herbinet, O.; Battin-Leclerc, F.; Bourgalais, J. Ozone-Assisted Oxidation of Ethylene in a Jet-Stirred Reactor: An Experimental and Modeling Study. *Chemical Physics Letters* 2022, *806*, 139986. https://doi.org/10.1016/j.cplett.2022.139986.
(11) Fan, H.; Ma, J.; Zhu, L.; Liu, B.; Liu, F.; Shan, X.; Wang, Z.; Wang, L. Unusual Diradical Intermediates in Ozonolysis of Alkenes: A Combined Theoretical and Synchrotron Radiation Photoionization Mass Spectrometric Study on Ozonolysis of Alkyl Vinyl Ethers. *J. Phys. Chem. A* 2022, *126* (43), 8021–8027. https://doi.org/10.1021/acs.jpca.2c04382.
(12) Rousso, A. C.; Hansen, N.; Jasper, A. W.; Ju, Y. Low-Temperature Oxidation of Ethylene by Ozone in a Jet-Stirred Reactor. *J. Phys. Chem. A* 2018, *122* (43), 8674–8685. https://doi.org/10.1021/acs.jpca.8b06556.
(13) Yang, S.; Wang, Q.; Curran, H. J.; Jia, M. Development of a 5-Component Gasoline Surrogate Model Using Recent Advancements in the Detailed H2/O2/CO/C1-C3 Mechanism for Decoupling Methodology. *Fuel* 2021, *283*, 118793.
(14) Cancino, L. R.; da Silva Jr, A.; De Toni, A. R.; Fikri, M.; Oliveira, A. A. M.; Schulz, C.; Curran, H. J. A Six-Compound, High Performance Gasoline Surrogate for Internal Combustion Engines: Experimental and Numerical Study of Autoignition Using High-Pressure Shock Tubes. *Fuel* 2020, *261*, 116439.
(15) Yuan, H.; Chen, Z.; Zhou, Z.; Yang, Y.; Brear, M. J.; Anderson, J. E. Formulating Gasoline Surrogate for Emulating Octane Blending Properties with Ethanol. *Fuel* 2020, *261*, 116243.
(16) Schönborn, A.; Hellier, P.; Ladommatos, N.; Hulteberg, C. P.; Carlström, G.; Sayad, P.; Klingmann, J.; Konnov, A. A. 1-Hexene Autoignition Control by Prior Reaction with Ozone. *Fuel Processing Technology* 2016, *145*, 90–95. https://doi.org/10.1016/j.fuproc.2016.01.029.
(17) Meng, X.; Rodriguez, A.; Herbinet, O.; Wang, T.; Battin-Leclerc, F. Revisiting 1-Hexene Low-Temperature Oxidation. *Combustion and Flame* 2017, *181*, 283–299. https://doi.org/10.1016/j.combustflame.2017.03.031.
(18) Griffiths, J. F. Negative Temperature-Coefficient of Reaction Rate during Hydrocarbon

Oxidation. *Journal of the Chemical Society D: Chemical Communications* 1969, No. 9, 483b–4484.
(19) Salooja, K. C. Zone of Negative Temperature Coefficient in Hydrocarbon Oxidation. *Nature* 1960, *185* (4705), 32–33. https://doi.org/10.1038/185032a0.
(20) Zhu, L.; Xu, Q.; Liu, B.; Xie, C.; Li, Y.; Wang, H.; Lou, H.; Zhu, Q.; Panigrahy, S.; Curran, H.; Wang, Z.; Ju, Y.; Wang, Z. Ozone-Assisted Low-Temperature Oxidation of Methane and Ethane. *Proceedings of the Combustion Institute* 2022, S1540748922004278. https://doi.org/10.1016/j.proci.2022.09.052.
(21) Herbinet, O.; Dayma, G. Jet-Stirred Reactors. In *Cleaner Combustion*; Battin-Leclerc, F., Simmie, J. M., Blurock, E., Eds.; Green Energy and Technology; Springer London: London, 2013; pp 183–210. https://doi.org/10.1007/978-1-4471-5307-8_8.
(22) Linstrom, P. J.; Mallard, W. G.; Eds. *NIST Chemistry WebBook, NIST Standard Reference Database Number 69*. National Institute of Standards and Technology, Gaithersburg MD, 20899 (accessed 2023-01-10).
(23) Scanlon, J. T.; Willis, D. E. Calculation of Flame Ionization Detector Relative Response Factors Using the Effective Carbon Number Concept. *Journal of Chromatographic Science* 1985, *23* (8), 333–340. https://doi.org/10.1093/chromsci/23.8.333.
(24) Jian, J.; Hashemi, H.; Wu, H.; Jasper, A. W.; Glarborg, P. A Reaction Mechanism for Ozone Dissociation and Reaction with Hydrogen at Elevated Temperature. *Fuel* 2022, *322*, 124138. https://doi.org/10.1016/j.fuel.2022.124138.
(25) Avzianova, E. V.; Ariya, P. A. Temperature-Dependent Kinetic Study for Ozonolysis of Selected Tropospheric Alkenes. *International journal of chemical kinetics* 2002, *34* (12), 678–684.
(26) Smith Lewin, C.; Kumar, A.; Herbinet, O.; Arnoux, P.; Asgher, R.; Barua, S.; Battin-Leclerc, F.; Farhoudian, S.; Garcia, G. A.; Tran, L.-S.; Vanhove, G.; Nahon, L.; Rissanen, M.; Bourgalais, J. 1-Hexene Ozonolysis Across Atmospheric and Combustion Temperatures via Synchrotron-Based Photoelectron Spectroscopy and Chemical Ionization Mass Spectrometry. *Submitted to The Journal of Physical Chemistry A* 2024.
(27) Kee, R. J.; Rupley, F. M.; Miller, J. A.; Coltrin, M. E.; Grcar, J. F.; Meeks, E.; Moffat, H. K.; Lutz, A. E.; Dixon-Lewis, G.; Smooke, M. D. CHEMKIN-PRO 15112, Reaction Design: San Diego, 2011.
(28) Rousso, A. C.; Hansen, N.; Jasper, A. W.; Ju, Y. Low-Temperature Oxidation of Ethylene by Ozone in a Jet-Stirred Reactor. *J. Phys. Chem. A* 2018, *122* (43), 8674–8685. https://doi.org/10.1021/acs.jpca.8b06556.
(29) Jian, J.; Hashemi, H.; Wu, H.; Glarborg, P. Study of Ammonia Oxidation with Ozone Addition. *Applications in Energy and Combustion Science* 2023, *14*, 100137. https://doi.org/10.1016/j.jaecs.2023.100137.
(30) Liao, H.; Kang, S.; Hansen, N.; Zhang, F.; Yang, B. Influence of Ozone Addition on the Low-Temperature Oxidation of Dimethyl Ether in a Jet-Stirred Reactor. *Combustion and Flame* 2020, *214*, 277–286. https://doi.org/10.1016/j.combustflame.2019.12.036.
(31) Rousso, A. C.; Jasper, A. W.; Ju, Y.; Hansen, N. Extreme Low-Temperature Combustion Chemistry: Ozone-Initiated Oxidation of Methyl Hexanoate. *J. Phys. Chem. A* 2020, *124* (48), 9897–9914. https://doi.org/10.1021/acs.jpca.0c07584.
(32) Namysl, S.; Pelucchi, M.; Herbinet, O.; Frassoldati, A.; Faravelli, T.; Battin-Leclerc, F. A First Evaluation of Butanoic and Pentanoic Acid Oxidation Kinetics. *Chemical Engineering Journal* 2019, *373*, 973–984. https://doi.org/10.1016/j.cej.2019.05.090.
(33) Bourgalais, J.; Smith Lewin, C.; Herbinet, O.; Garcia, G. A.; Arnoux, P.; Tran, L.-S.;

507 Vanhove, G.; Nahon, L.; Battin-Leclerc, F. Refining the Chain-Branching Process in the Low-
508 Temperature Oxidation of 1-Hexene with Synchrotron-Based PEPICO Spectroscopy. *Combustion*
509 *and Flame* 2023, *258*, 113065. https://doi.org/10.1016/j.combustflame.2023.113065.
510

511 **TOC GRAPHIC**

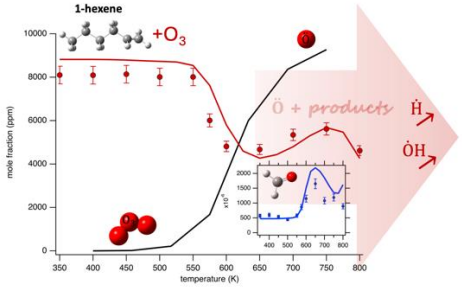

512